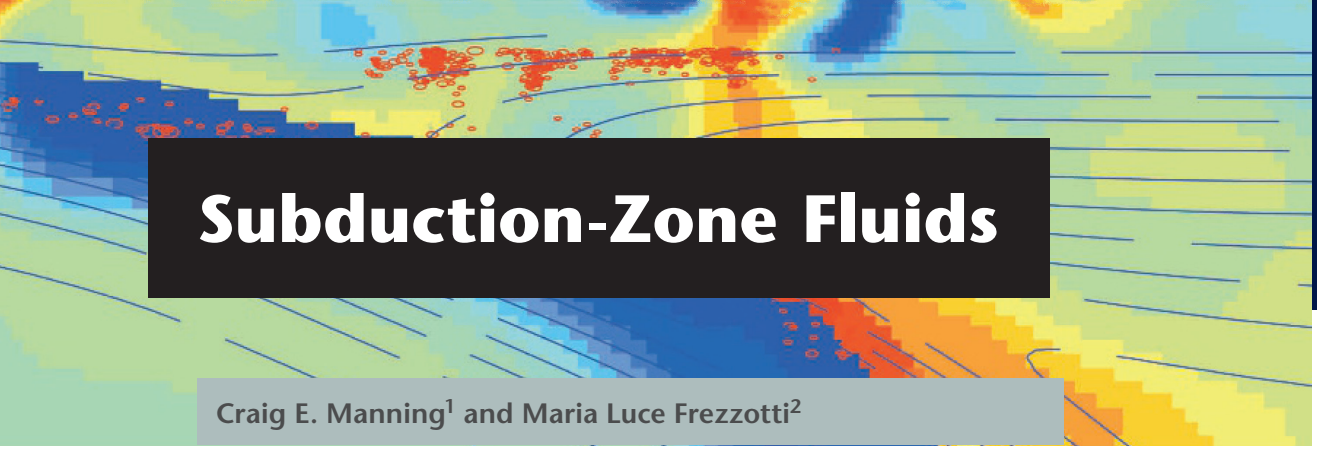

Subduction-Zone Fluids

Craig E. Manning[1] and Maria Luce Frezzotti[2]

1811-5209/20/0016-0395$2.50 DOI: 10.2138/gselements.16.6.395

Fluids are essential to the physical and chemical processes in subduction zones. Two types of subduction-zone fluids can be distinguished. First, shallow fluids, which are relatively dilute and water rich and that have properties that vary between subduction zones depending on the local thermal regime. Second, deep fluids, which possess higher proportions of dissolved silicate, salts and non-polar gases relative to water content, and have properties that are broadly similar in most subduction systems, regardless of the local thermal structure. We review key physical and chemical properties of fluids in two key subduction-zone contexts—along the slab top and beneath the volcanic front—to illustrate the distinct properties of shallow and deep subduction-zone fluids.

KEYWORDS: fluids, subduction, volcanic arcs, metamorphism, aqueous geochemistry

INTRODUCTION

Fluids play a critical role in subduction-zone processes, from the trench to well beyond sub-arc depths, and perhaps even to the mantle transition zone. Fluid release during metamorphism may produce intermediate-depth earthquakes, slow slip and tremor (Hacker et al. 2003; Kodaira et al. 2004; Zhan 2020) while transporting heat (Spinelli and Wang 2009) and explaining electrical conductivity patterns in the slab and the mantle wedge (Pommier and Evans 2017). Subduction-zone fluids (SZFs) also have profound chemical effects. Primitive arc magmas contain elevated concentrations of the main components of SZFs, a hallmark of their participation in the melting of the mantle wedge (e.g., Ulmer 2001), and SZFs play a central role in element cycles.

The geologic record is replete with evidence for fluids in rocks exhumed from subduction zones (Bebout and Penniston-Dorland 2016). Metamorphic minerals host fluid inclusions that contain H_2O, along with salts, non-polar gases (e.g., CO_2, CH_4 and N_2) and other dissolved rock components (e.g., Frezzotti and Ferrando 2015). Metamorphic veins represent minerals precipitated from SZFs at a range of conditions; trace element and isotope geochemistry offer strong evidence for fluid–rock interaction deep in subduction zones (Bebout and Penniston-Dorland 2016).

There have been numerous previous reviews of SZFs, chiefly focused on compositions and chemistry (Manning 2004; Sanchez-Valle 2013; Frezzotti and Ferrando 2015; Bebout and Penniston-Dorland 2016; Ni et al. 2017). Reviews of "fluids" at subduction-zone conditions are complicated by the vast array of compositional possibilities: an SZF may be dominated by H_2O, other gases, salts, or rock components. Subduction *P–T* paths may produce fluid-saturated melting of certain lithologies, and such melts may vary continuously in composition from silicate- or carbonate-rich liquids to fluids rich in low-density components (e.g., H_2O, CO_2). Here, we discuss fluid properties independent of whether or not a particular *P–T* path, bulk composition or thermodynamic model predicts the presence of a separate, discrete silicate melt phase. Hence, our focus is on the properties of fluids comparatively rich in low-density components, even though the activities of these components may be low. In addition, we do not discuss the shallow expulsion of entrained pore water or the fluids generated during continental subduction (e.g., Hermann et al. 2013). We first distinguish two broad classes of SZF based on composition, and then compare and contrast their depth-dependent properties. We show how property variations influence subduction-zone processes at a range of depths.

ENVIRONMENTAL CONTROLS ON SUBDUCTION-ZONE FLUIDS

FIGURE 1A shows a schematic cross section of an ocean–continent convergent margin, with a superimposed thermal model for the Alaska Peninsula (Syracuse et al. 2010). At depths greater than ~20 km, SZFs are produced by metamorphic transformation of minerals containing fluid components such as H_2O (as OH groups or molecular H_2O), CO_2 (as carbonate), and salts (chiefly as structurally bound alkalis and Cl). The properties of these fluids are ultimately controlled by the temperature–depth structure of the local subduction system.

The temperature–depth pattern in FIGURE 1A is characteristic of subduction zones, where relatively cool temperatures in the slab persist to great depth due to the low thermal diffusivity of rocks relative to tectonic transport rates. The mechanical transition from a shallow regime in which the slab and overlying mantle are decoupled, to a deeper regime in which they are coupled implies that temperatures near the slab top increase substantially over the relatively

1 Department of Earth, Planetary and Space Sciences
University of California Los Angeles
Los Angeles CA, 90095-1567, USA
E-mail: manning@epss.ucla.edu

2 Dipartimento Scienze dell'Ambiente e della Terra
Università di Milano – Bicocca
20126 Milano, Italy
E-mail: maria.frezzotti@unimib.it

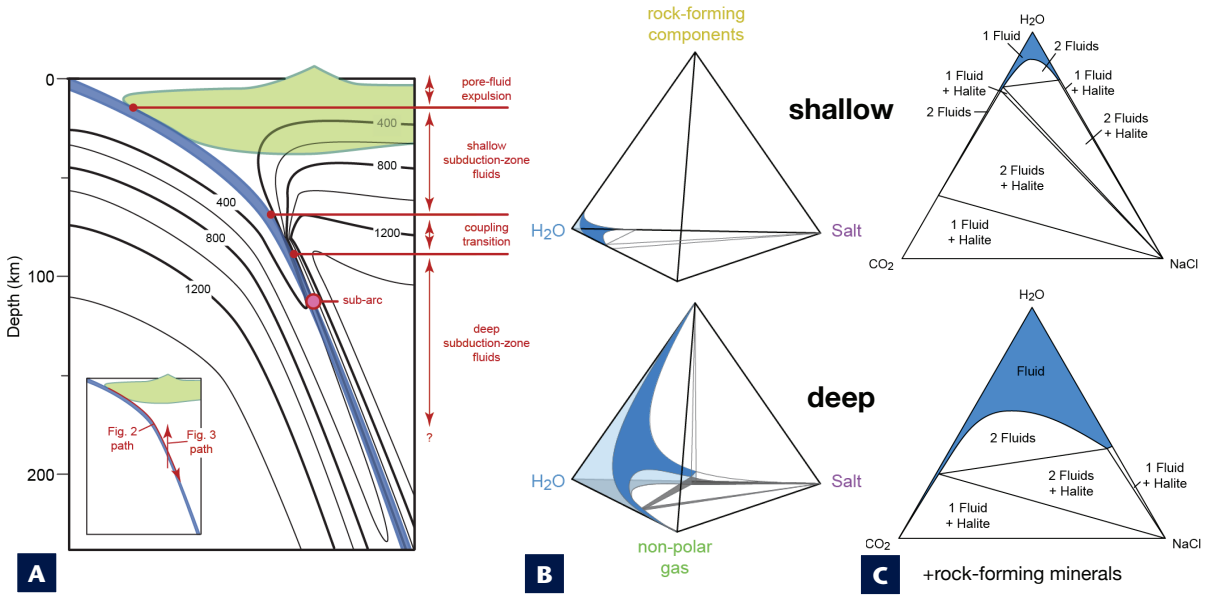

Figure 1 (**A**) Schematic cross section of the Alaska Peninsula (USA) subduction zone, an example of an ocean–continent subduction system. Isotherms from the D80 model of Syracuse et al. (2010). The crust in the upper plate is ~35 km thick; the ocean crust + sediment package is 7 km thick; the depth to the slab beneath the arc (circle labeled "sub-arc") is 108 km. **Inset** The slab-top and vertical sub-arc temperature–depth paths used in Figures 2 and 3, respectively. In the upper reaches of a subduction zone, fluids are chiefly entrained as pore fluids in sediments and, to a lesser extent, in the upper oceanic crust. They are mostly expelled by compaction by a depth of ~20 km. At greater depths, subduction-zone fluids (SZFs) are secondary, derived from metamorphic devolatilization. The characteristic thermal structure of subduction zones leads to distinct differences between shallow (~20–70 km) and deep (>90 km) SZFs, with a narrow ~20 km transition. The depth intervals of shallow and deep fluids may vary depending on the nature of mechanical coupling of the slab and mantle wedge (see text). (**B**) Compositional characteristics of the two types of fluids. Apices of quaternary diagrams are H_2O, non-polar gas (e.g., CO_2), salt (e.g., NaCl), and rock-forming minerals (chiefly silicates). Dark blue surfaces show fluid compositions coexisting with rock-forming minerals, and schematically illustrate that the two fluid types differ in solute concentration. Light-blue volumes show the range of stable fluid compositions in the absence of rock. After Manning (2018). (**C**) Compositions of fluids coexisting with rock-forming minerals projected onto the basal triangles in Figure 1B, assuming CO_2 and NaCl are the gas and salt components. Region of stability of a single H_2O–NaCl–CO_2 fluid is shown in blue; other regions involving additional phases are uncolored. The term "fluid" is used regardless of density. Because fluids reside in rock porosity, consideration of hydrothermal properties should, where possible, account for the effects of the widely ranging, depth-dependent solute load. Consideration only of the compositions on the H_2O–gas–salt base of diagrams in Figure 1B can be problematic.

narrow depth range of transition (e.g., Syracuse et al. 2010). This can be seen in temperature–depth relations for model cool subduction zones (e.g., Central Honshu off Japan), intermediate subduction zones [e.g., Alaska Peninsula off Alaska (USA)], and warm subduction zones [e.g., off Cascadia, from southern Canada to California (USA)] (Fig. 2A). Regardless of the thermal regime, the temperature rises slowly to the depth of the coupling transition where it then increases by several hundred degrees over a few kilometers. Temperature increase with depth is not as great below this zone.

The accuracy of the predicted temperatures at shallow depths and of the large temperature change associated with coupling is a matter of debate. Metamorphic rocks exhumed from <80 km record higher temperatures (Fig. 2A) (Penniston-Dorland et al. 2015). Possible explanations are shear heating at the slab top or that exhumed rocks record an early, higher-*T* stage of subduction (van Keken et al. 2018). Regardless, the weight of geophysical evidence favors some sort of thermal inflection associated with coupling. Therefore, for the purposes of this paper, we use the models developed by Syracuse et al. (2010), with a constant 80 km depth of coupling, for investigating the properties of SZFs. Our conclusions are largely independent of the choice of subduction-zone thermal models.

TWO TYPES OF SUBDUCTION-ZONE FLUID

Along the slab top, the temperature change with depth differs above and below the coupling transition (Fig. 2A). This leads to two broadly different SZFs: shallow and deep. The distinction is made using the geothermal gradient along the slab top, because this boundary is responsible for many of the profound chemical and physical effects of a given SZF. As shown qualitatively in Figures 1B and 1C, shallow fluids tend to be relatively dilute and water-rich, with low overall solubility of silicate material, salt and non-polar gases such as CO_2. In contrast, deep fluids can have a very high concentration of rock components, salts and gases: in some cases, properties and compositions may merge with those of rock melts. The abundance of other components reduces H_2O activity so that deep SZFs may exist at temperatures and depths greater than those at which some subducted lithologies melt in the presence of pure H_2O (diamond symbols in Fig. 2A,). Below, we examine SZF properties at the slab top and across the slab–mantle interface beneath volcanic arcs.

The H_2O in Subduction-Zone Fluid Along a Slab Top

The properties of the H_2O component of SZFs dominate the overall fluid properties along subduction paths and, therefore, provide a useful, if simplistic, starting point for this survey. Water density steadily rises from the trench to ~75 km depth (Fig. 2B). However, the large temperature increase at 75–85 km leads to an along-slab inversion in the fluid density gradient that could affect fluid flow paths. Any effect is limited to the sediment and upper basalt layers of the subducting lithosphere. Below the transition region, H_2O density again increases with depth.

The dielectric constant measures a solvent's ability to shield the electrical fields of ions. The dielectric constant of water (ε_{H_2O}) is often taken as a proxy for the extent of dissociation of dissolved salts. Higher ε_{H_2O} means greater shielding,

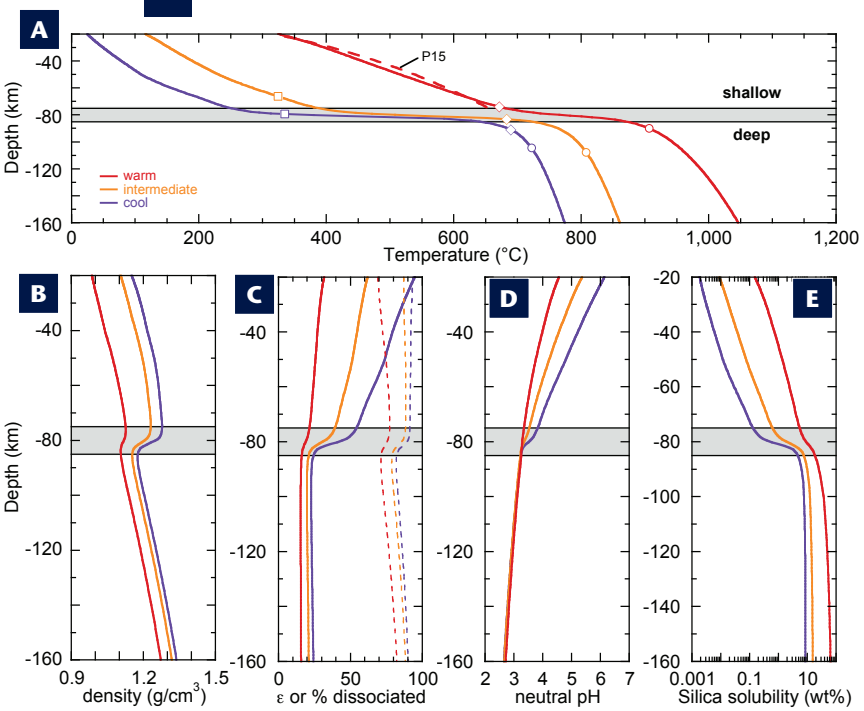

Figure 2 (**A**) Temperature–depth curves for the slab top beneath the central portion of Honshu (Japan) (purple), representing cool subduction zones; the Alaskan Peninsula (USA) (orange), representing intermediate subduction zones; and Cascadia (northwest USA) (red) representing warm subduction zones. The grey shaded region represents the depth range of the transition from shallow (above) to deep (below) subduction-zone fluids (SZFs). Dashed red curve labeled "P15" is the geotherm for exhumed metamorphic rocks (Penniston-Dorland et al. 2015) and, shallower than ~80 km, is similar to warm slab-top geotherms. Open circles indicate the point on the slab top directly below the volcanic front. Diamonds show where average slab sediment melts in the presence of pure H_2O (Hermann et al. 2013); melting points shift to greater depth with decreasing H_2O activity in deep SZFs (see text). Squares denote crest of the H_2O–CO_2 miscibility gap (Abramson et al. 2017), i.e., the maximum depth to which two coexisting fluid phases can coexist in the binary system (encountered on the Honshu and Alaska paths). After Syracuse et al. (2010), using D80 models. (**B**) The density of H_2O vs. depth. (**C**) The dielectric constant of H_2O (solid lines) and the percent dissociation of 1 molal NaCl solution (dashed lines) vs. depth. (**D**) Neutral pH in H_2O vs. depth. (**E**) The SiO_2-mineral solubility (quartz or coesite) vs. depth. Colours and shading for lower panels as for Figure 1A. After Zhang and Duan (2005) and Huang and Sverjensky (2019).

favoring ion stability and rightward progress of reactions among dissolved components, such as $NaCl_{aq} = Na^+ + Cl^-$. Along the slab-top geotherms, ε_{H_2O} declines steadily with depth (Fig. 2C). The dielectric constant decreases strongly in the mechanical coupling transition. At greater depths, ε_{H_2O} is uniformly ~20 ± 5 and shows little depth dependence. The patterns might seem to imply reduced solute ionization with depth, but the extent of solute dissociation is not so simple: a 1 molal (5.5 wt%) NaCl solution is >70% dissociated along all slab-top geotherms (Fig. 2C), and dissociation extent actually *increases* with depth in deep SZFs. This is because, relative changes aside, ε_{H_2O} at all conditions is still too high for extensive ion-pairing in dilute solutions, which becomes pronounced at ε_{H_2O} <10. Thus, at modest concentrations, salts remain mostly dissociated along slab-top geotherms. The extent of association increases as salt concentration rises.

Neutral pH (pH_n) displays a pattern similar to ε_{H_2O} (Fig. 2D). It declines in shallow SZFs, and there are distinct differences between subduction zones. However, pH_n values converge in the transition region, and together show minimal depth dependence in all deep fluids. The low pH_n of 3.0 ± 0.5 in deep SZFs is a signal of a greater extent of H_2O dissociation, so that H^+ and OH^- contribute significantly to the ionic strength. This decreases ion activity coefficients, which further promotes ion dissociation and more extensive mineral dissolution. Hence, greater water dissociation leads naturally to higher mineral solubility, pointing to higher solute concentrations in deep SZFs (see below).

The distinction between the properties of shallow and deep SZFs is most pronounced near the slab top: in the subducting sediments and in the upper oceanic crust. In the subducting lower crust and mantle lithosphere, the differences between shallow and deep fluids are expressed by less extreme changes in slopes of the property versus depth curves.

The H_2O in Subduction-Zone Fluid Beneath an Arc Front

Upward flow of deep SZFs from the slab into the wedge beneath the volcanic arcs is important for processes associated with mantle-wedge metasomatism and magma generation. For example, the slab depth beneath the Alaska Peninsula arc front is ~108 km (Fig. 3A). Along a vertical transect starting at the thermal minimum of ~400 °C and at –124 km in down-going mantle lithosphere, the temperature rises to ~800 °C at the slab–mantle interface, then to a thermal maximum of 1,410 °C at –89 km in the mantle wedge.

The temperature rise of ~27 °C/km along this vertical path has profound consequences for the properties of aqueous fluids derived from the slab. Water density decreases from

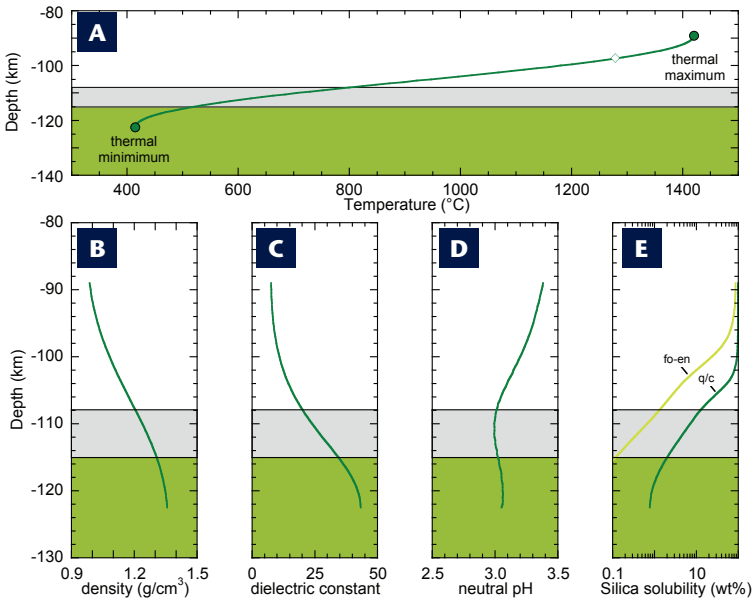

Figure 3 (**A**) Temperature–depth curve for the depth interval near the slab–mantle interface, Alaskan Peninsula, highlighting the region of inverted thermal gradient. The gray shaded region corresponds to sediment and oceanic crust in the subducting slab, uncolored is mantle wedge, green is subducting mantle lithosphere. Green diamond shows depth of melting (enstatite + H_2O = forsterite + liquid) on the geotherm; melting shifts to shallower depths with decrease in H_2O activity. After Syracuse et al. (2010), using D80 model. (**B**) The density of H_2O vs. depth. (**C**) The dielectric constant of H_2O vs. depth. (**D**) Neutral pH in H_2O vs. depth. (**E**) The aqueous SiO_2 concentration vs. depth in equilibrium with SiO_2 minerals [quartz/coesite (q/c), dark green] is contrasted with that with forsterite + enstatite ("fo-en", light green).

~1.4 g/cm^3 to <1.0 g/cm^3 (Fig. 3B), producing a driving force (dP_{fluid}/dz) for vertical flow that increases from ~0.19 bar/m to 2.3 bar/m. This favors vertical fluid flow from slab to wedge; the dielectric constant drops to <10, favoring salt association; and pH_n increases into the mantle wedge (Figs. 3C, 3D).

The H_2O–Silicate System in Subduction-Zone Fluids

While the properties of H_2O are critical for understanding the behavior of fluids in subduction zones, slab metamorphism yields additional volatiles, salts and rock-derived components (Fig. 1). Consider first the interactions between H_2O and silicate components. Slab fluids are sourced in, or equilibrate with, metasediment and metabasalt, which are saturated with quartz or coesite, silica being typically the most abundant locally derived solute in high *P*–*T* fluids (e.g., Manning 2018). Accordingly, a reasonable picture of the overall solute load can be obtained simply from the solubility of the SiO_2 minerals alone.

Dissolved silica concentration in H_2O saturated with quartz or coesite increases with depth (Fig. 2E). Shallow SZFs differ strongly depending on thermal regime: at depths of slab–mantle coupling, SiO_2 concentrations range from ~0.1 wt% (Honshu) to ~5 wt% (Cascadia). Silica contents are higher and change less with depth in deep SZFs. In this case, deep SZFs exhibit differences depending on thermal regime due to the strong temperature dependence of solubility. Silica concentration in deep coesite-saturated fluids is up to ~9 wt% in Honshu, ~15 wt% in the Alaska Peninsula, and ~70 wt% in Cascadia.

In the sub-arc region, silica solubility increases dramatically along a vertical flow path due to the strong thermal gradient. The decompressing and heating of slab fluids will help dissolve progressively more SiO_2, reaching 12.5 wt% at the mantle contact. The interface is an important boundary because of silica undersaturation in the ultramafic mantle wedge. A model harzburgite requires silica concentration to be 1.3 wt% via buffering by the following equilibrium:

$$Mg_2SiO_4 + SiO_{2aq} = 2MgSiO_3 \quad [1]$$

forsterite enstatite

Thus, the requisite drop in silica concentration may yield metasomatic modification of the mantle wedge as aqueous silica reacts with olivine to produce relatively SiO_2-rich orthopyroxene. The orthopyroxene mode and whole-rock SiO_2 will tend to increase with the loss of olivine. Mantle-wedge rocks with elevated modes of silica-rich minerals are a hallmark of slab-fluid metasomatism.

Though we consider only silica, the example highlights the profound metasomatic power of slab fluids. Figure 4A illustrates the amount of fluid needed to convert a model MgO–SiO_2 sub-arc column of harzburgite (85 vol% forsterite, 15 vol% enstatite) to 100% enstatite (orthopyroxenite). A fluid/rock mass ratio of 120:1 would convert the entire mantle-wedge column to enstatite to the depth of the wet solidus in the model system. But this is likely a significant overestimate of the amount of fluid needed. Silica enrichment of the mantle wedge probably occurs updip as well, and downward mantle flow would supply already metasomatized rock to the sub-arc column. Updip modification to 50% or more enstatite would require a fluid/rock ratio of <60 to complete the conversion beneath the arc (Fig. 4A).

A subduction-zone fluid that is interacting with sediments at the slab top will be more complicated due to additional components. The *P* and *T* at the slab top directly beneath the volcanic arcs (Syracuse et al. 2010) are shown in Figure 4B, along with a slab-sediment–H_2O phase diagram (Hermann et al. 2013) and the model slab-top geotherms. Slab-top conditions beneath arcs are very near the second critical end point on the melting curve. At *P* above this point, sediment dissolves continuously in H_2O with no

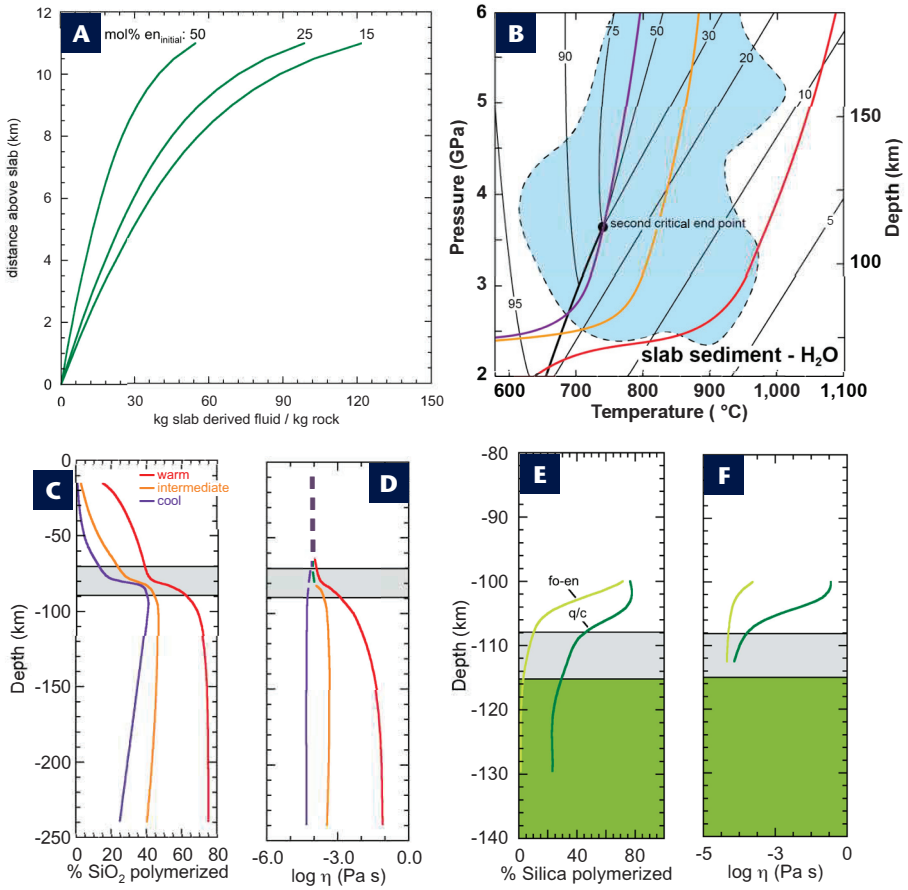

Figure 4 (**A**) Mass ratio of slab-derived SiO_2–H_2O fluid (coesite saturated) required to convert model harzburgite to 100% enstatite (Reaction 1 in text), for starting initial enstatite ($en_{initial}$) of 15, 25 and 50 mol%, where 15% reflects model unmodified harzburgite, and 25 mol% and 50 mol% account for up-dip silica metasomatism. (**B**) Pressure–temperature projection of hydrous melting of model slab sediment (bold black line), with H_2O isopleths (in wt%) and second critical end point on the melting curve (filled circle). Filled region (blue) shows range of slab-top *P*–*T* points beneath the volcanic front in subduction zones studied by Syracuse et al. (2010): all models, except Tonga (T550) and Kermadec (X25) have been omitted. Purple, orange, and red curves show *P*–*T* paths of representative subduction zones (see Figs. 2 and 3). After Hermann et al. (2013). (**C**) Graph of %SiO_2 polymerized vs. depth along representative slab-top geotherms. Polymerization SiO_2 calculated using data from Sverjensky et al. (2014) and Huang and Sverjensky (2019) (**D**) Graph of log viscosity (Pa S) vs. depth along representative slab-top geotherms. Viscosity of SiO_2–H_2O fluid approximated using model of Audetat and Keppler (2004) between 600°C and 1,200°C; dashed where extrapolated. (**E**) Graph of % SiO_2 polymerized vs. depth near slab top beneath volcanic front. Dark vs. light green lines show silica polymerization in H_2O saturated with quartz/coesite (q/c) and enstatite + forsterite (fo-en), respectively. (**F**) Graph of log viscosity vs. depth near slab top beneath volcanic front. Dark and light green lines as for Figure 4E.

discreet melting. Hints of this behavior are captured in Figures 2E and 3E, which show >70–90 wt% SiO_2 near or above this pressure. This behavior arises from progressive solute polymerization, as in hydrous silicate liquids (Manning 2004; Manning et al. 2010). In shallow SZFs, polymeric silica (dimers and trimers) is a small fraction of total dissolved silica except in the hottest subduction zones (Fig. 4C). However, in deep SZFs, polymerized silica can have a wide range of concentrations: it is always >20% and may predominate at high temperature. Beneath arcs, silica polymerization increases to nearly 80% in ascending fluids (Fig. 4E).

High solute concentration and polymerization yield elevated density and viscosity (Audetat and Keppler 2004; Hack and Thompson 2011). Audetat and Keppler (2004) found little effect of composition on viscosity, so we use their model to approximate the viscosities of SiO_2–H_2O fluids. Fluid viscosity decreases by many orders of magnitude with the addition of small amounts of H_2O to dry melts due to the disruption of network-forming components; however, above ~40 wt% H_2O there is only a small further viscosity decrease with additional water. Viscosities of shallow SZFs and cold, deep SZFs are similar to pure H_2O, ~10^{-4} Pa s, but are higher in the deep SZFs of intermediate and hot subduction zones where solute loads are elevated (Fig. 4D). Viscosities decline on vertical paths beneath arcs, and there is a large viscosity drop upon entering the mantle wedge due to the abrupt change in fluid composition at the slab-mantle interface (Fig. 4F).

Salt and Gas Components in a Subduction-Zone Fluid

Non-polar gases such as CO_2 and salts such as NaCl are important components of SZFs (Frezzotti and Ferrando 2015; Keppler 2017; Barnes et al. 2018). The properties of pure fluids (H_2O, CO_2, etc.) vary smoothly along subduction *P*–*T* paths. However, mixtures along binaries are more complex. Whereas H_2O–NaCl fluids are fully miscible to halite saturation (Fig. 1), H_2O–CO_2 fluids can unmix in shallow SZFs along low to intermediate slab-top gradients (Abramson et al. 2017). In deep SZFs, the contrasting properties of H_2O–gas and H_2O–salt mixtures (e.g., Manning 2018) lead to substantial immiscibility in the ternary system (Figs. 1B and 1C). Where gas and salt concentrations are high, not only can water activity be sufficiently suppressed to hinder melting, but also two discreet fluids—one a brine, the other rich in gases—may separate and migrate independently. The properties of such fluid mixtures are poorly known, so below we focus on single-phase fluids along binaries with H_2O.

In general, fluid densities along slab-top geotherms will show the same relative changes as for pure H_2O. Added CO_2 and/or NaCl decreases the bulk dielectric constant at a given *P* and *T* (e.g., Manning 2018) but, as with density, the relative changes in dielectric constant with depth are similar to pure H_2O. Thus, relative variations in density and dielectric constant of an SZF with depth in a subduction zone can be expected to be largely independent of added gas and salt components.

Perhaps the most significant effects of salt or gas addition to an SZF involves mineral solubility and electrical conductivity. The presence of CO_2 and NaCl have complex consequences for the solubility of rock-forming silicates (Manning 2018; Macris et al. 2020), but insufficient data exist to quantify the effects over the pressure range needed. Non-polar gases are poor solvents for silicates and oxides so, in general, the higher the gas concentration, the lower the solute load. Salt (NaCl) has a similar effect on SiO_2, but interactions between Cl and metals leads to an elevation of solubility for key mantle minerals (e.g., Macris et al. 2020). Carbonate minerals show strong increases in solubility in H_2O with depth in a subduction zone (Frezzotti et al. 2011; Kelemen and Manning 2015), and this effect is enhanced by added salt (Manning 2018).

Electromagnetic surveys reveal that electrical conductivity is commonly elevated near the slab–mantle interface in subduction zones (Fig. 5A) (Pommier and Evans 2017). For example, there is a zone of high conductivity at the slab–mantle interface and in the mantle wedge of Cascadia at 40 ± 10 km depth (Fig. 5A). The addition of non-polar gases will generally decrease conductivity, except where

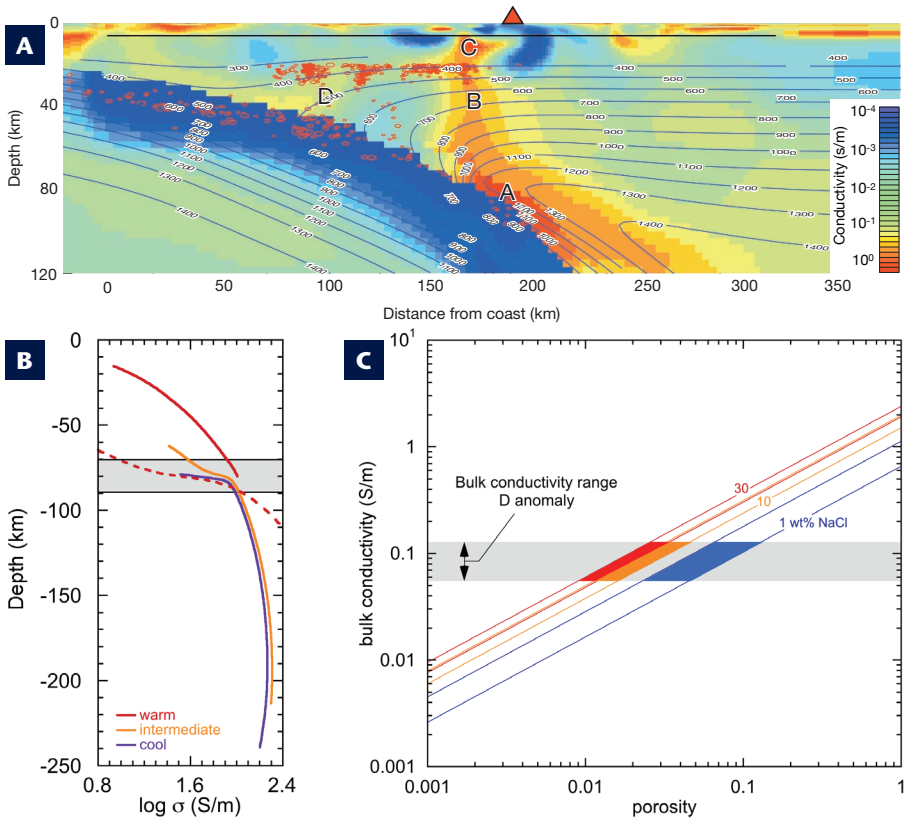

Figure 5 (**A**) Magnetotelluric model for the Cascadia subduction system. Numbered contours = temperature in °C; red circles = earthquake hypocenters; red triangle = arc front (Mt. Rainier). Regions labeled B, C, D are high-conductivity anomalies. After McGary et al. (2014). (**B**) Log conductivity (Siemens per meter, S/m) of 5 wt% NaCl solution along slab-top geotherms for cool, intermediate and warm subduction systems (colors as in Fig. 2). Red dashed curve is approximate conductivity of H_2O in equilibrium with aragonite along the Cascadia geotherm, assuming dissolved carbonate conductivity can be modeled like NaCl. After Kelemen and Manning (2015) and Manning (2018). (**C**) Porosity vs. bulk conductivity plot showing range of porosities required to explain bulk conductivities associated with region D anomaly at 40 ± 10 km in Figure 5A (grey shaded region). Results for 1, 10, and 30 wt% NaCl shown in blue, orange, and red, respectively. In each, the lower line shows calculation at 30 km, upper line at 50 km depth along the Cascadia slab-top geotherm. Bulk conductivity (s_b) calculated using Archie's Law ($s_b = s_f f^m$, where s_f is fluid conductivity, ϕ is porosity, and *m* is 0.8).

interactions with H_2O yield ionic species such as carbonate ions. In contrast, the addition of salts, such as NaCl, yields strong increases in conductivity (Guo and Keppler 2019), while also promoting fluid migration. Figure 5B shows that electrical conductivity of a 5 wt% NaCl solution increases by >10 times with depth along the slab–mantle interface. However, for such a fluid to explain the observed bulk conductivity of ~10^{-1} S/m (Fig. 5A), a very high and likely unrealistic rock porosity of >5% is required (Fig. 5C). In contrast, salinities of >10 wt% yield the observed conductivity at a lower, and more reasonable, porosity. The fact that the conductivity anomalies extend into the mantle wedge, but the slab itself has low conductivity, may suggest reaction enhancement of salinity via a process such as serpentinization (i.e., H_2O consumption). The very high conductivities beneath an arc front probably results from a complex mixture of melt and fluid. Notably, alkali halides are not the only path to raising the conductivity of SZFs. The rise in solubility of $CaCO_3$ minerals in H_2O translates to substantial electrolyte concentrations (e.g., HCO_3^-), and, therefore, high conductivity. Figure 5B shows that ions derived from carbonate minerals could be very important, especially at sub-arc depths.

CONCLUDING REMARKS

We distinguish two broad types of subduction-zone fluid. Shallow fluids are relatively dilute, and properties tend to vary among subduction zones and to depend on the local thermal structure. Deep fluids may have higher concentrations of salts, gases and rock components; their properties are more similar across the global range of subduction types. Deep fluids are especially important in the sub-arc region, where there is a strong pressure drive for upward vertical flow and where associated heating leads to large gradients in properties and metasomatic capability. Chemical changes in concentrated silicate solutes are expressed in viscosity variations. And elevated salt concentrations can explain the zones of electrical conductivity that are evident in many subduction zones.

ACKNOWLEDGMENTS

The manuscript was prepared while CEM benefited from the generous support of the Institut de Physique du Globe de Paris (France). We thank Huaiwei Ni and Joerg Hermann for insightful, constructive reviews. The work was supported by National Science Foundation grant EAR-1732256 to CEM and by Ministero dell'Istruzione dell'Università e della Ricerca grant PRIN-2017LMNLAW and Progetto Dipartimenti di Eccellenza grant 2018-2022 to MLF.

REFERENCES

Abramson EH, Bollengier O, Brown JM (2017) The water-carbon dioxide miscibility surface to 450°C and 7 GPa. American Journal of Science 317: 967-989

Audétat A, Keppler H (2004) Viscosity of fluids in subduction zones. Science 303: 513-516

Barnes JD, Manning CE, Scambelluri M, Selverstone J (2018) The behavior of halogens during subduction-zone processes. In: Harlov D, Aranovich L (eds) The Role of Halogens in Terrestrial and Extraterrestrial Geochemical Processes. Springer, Cham, pp 545-590

Bebout GE, Penniston-Dorland SC (2016) Fluid and mass transfer at subduction interfaces—the field metamorphic record. Lithos 240-243: 228-258

Frezzotti ML, Ferrando S (2015) The chemical behavior of fluids released during deep subduction based on fluid inclusions. American Mineralogist 100: 352-377

Frezzotti ML, Selverstone J, Sharp ZD, Compagnoni R (2011) Carbonate dissolution during subduction revealed by diamond-bearing rocks from the Alps. Nature Geoscience 4: 703-706

Guo H, Keppler H (2019) Electrical conductivity of NaCl-bearing aqueous fluids to 900°C and 5 GPa. Journal of Geophysical Research: Solid Earth 124: 1397-1411

Hack AC, Thompson AB (2011) Density and viscosity of hydrous magmas and related fluids and their role in subduction zone processes. Journal of Petrology 52: 1333-1362

Hacker BR, Peacock SM, Abers GA, Holloway SD (2003) Subduction factory 2. Are intermediate-depth earthquakes in subducting slabs linked to metamorphic dehydration reactions? Journal of Geophysical Research: Solid Earth 108, doi: 10.1029/2001JB001129

Hermann J, Zheng Y-F, Rubatto D (2013) Deep fluids in subducted continental crust. Elements 9: 281-287

Huang F, Sverjensky DA (2019) Extended deep earth water model for predicting major element mantle metasomatism. Geochimica et Cosmochimica Acta 254: 192-230

Kelemen PB, Manning CE (2015) Reevaluating carbon fluxes in subduction zones, what goes down, mostly comes up. Proceedings of the National Academy of Sciences of the United States of America 112: E3997-E4006

Keppler H (2017) Fluids and trace element transport in subduction zones. American Mineralogist 102: 5-20

Kodaira S and 5 coauthors (2004) High pore fluid pressure may cause silent slip in the Nankai Trough. Science 304: 1295-1298

Macris CA, Newton RC, Wykes J, Pan R, Manning CE (2020) Diopside, enstatite and forsterite solubilities in H_2O and H_2O-NaCl solutions at lower crustal and upper mantle conditions. Geochimica et Cosmochimica Acta 279: 119-142

Manning CE (2004) The chemistry of subduction-zone fluids. Earth and Planetary Science Letters 223: 1-16

Manning CE (2018) Fluids of the lower crust: deep is different. Annual Review of Earth and Planetary Sciences 46: 67-97

Manning CE, Antignano A, Lin HA (2010) Premelting polymerization of crustal and mantle fluids, as indicated by the solubility of albite + paragonite + quartz in H_2O at 1 GPa and 350–620°C. Earth and Planetary Science Letters 292: 325-336

McGary RS, Evans RL, Wannamaker PE, Elsenbeck J, Rondenay S (2014) Pathway from subducting slab to surface for melt and fluids beneath Mount Rainier. Nature 511: 338-340

Ni H, Zhang L, Xiong X, Mao Z, Wang J (2017) Supercritical fluids at subduction zones: evidence, formation condition, and physicochemical properties. Earth-Science Reviews 167: 62-71

Penniston-Dorland SC, Kohn MJ, Manning CE (2015) The global range of subduction zone thermal structures from exhumed blueschists and eclogites: rocks are hotter than models. Earth and Planetary Science Letters 428: 243-254

Pommier A, Evans RL (2017) Constraints on fluids in subduction zones from electromagnetic data. Geosphere 13: 1026-1041

Sanchez-Valle C (2013) Structure and thermodynamics of subduction zone fluids from spectroscopic studies. Reviews in Mineralogy and Geochemistry 76: 265-309

Spinelli G, Wang K (2009) Links between fluid circulation, temperature, and metamorphism in subducting slabs. Geophysical Research Letters 36, doi: 10.1029/2009GL038706

Sverjensky DA, Harrison B, Azzolini D (2014) Water in the deep Earth: the dielectric constant and the solubilities of quartz and corundum to 60 kb and 1200°C. Geochimica et Cosmochimica Acta 129: 125-145

Syracuse EM, van Keken PE, Abers GA (2010) The global range of subduction zone thermal models. Physics of the Earth and Planetary Interiors 183: 73-90

Ulmer P (2001) Partial melting in the mantle wedge — the role of H_2O in the genesis of mantle-derived 'arc-related' magmas. Physics of the Earth and Planetary Interiors 127: 215-232

van Keken PE, Wada I, Abers GA, Hacker BR, Wang K (2018) Mafic high-pressure rocks are preferentially exhumed from warm subduction settings. Geochemistry, Geophysics, Geosystems 19: 2934-2961

Zhan Z (2020) Mechanisms and implications of deep earthquakes. Annual Review of Earth and Planetary Sciences 48: 147-174

Zhang Z, Duan Z (2005) Prediction of the *PVT* properties of water over wide range of temperatures and pressures from molecular dynamics simulation. Physics of the Earth and Planetary Interiors 149: 335